PAPER • OPEN ACCESS

Unified treatment of recoil and Doppler broadening in molecular high-energy photoemission

New Journal of Physics
The open access journal at the forefront of physics

Deutsche Physikalische Gesellschaft DPG
IOP Institute of Physics

Published in partnership with: Deutsche Physikalische Gesellschaft and the Institute of Physics

OPEN ACCESS

RECEIVED
7 April 2021

REVISED
3 June 2021

ACCEPTED FOR PUBLICATION
7 June 2021

PUBLISHED
24 June 2021

PAPER

Unified treatment of recoil and Doppler broadening in molecular high-energy photoemission

E Kukk[1], D Céolin[2], O Travnikova[2,3], R Püttner[4,*], M N Piancastelli[3,5], R Guillemin[2,3], L Journel[2,3], T Marchenko[2,3], I Ismail[3], J Martins[3], J-P Rueff[2,3] and M Simon[2,3]

[1] Department of Physics and Astronomy, University of Turku, FI-20014 Turku, Finland
[2] Synchrotron SOLEIL, L'Orme des Merisiers, Saint-Aubin, BP 48, FR-91192 Gif-sur-Yvette Cedex, France
[3] Sorbonne Université, CNRS, Laboratoire de Chimie Physique-Matière et Rayonnement, F-75005 Paris, France
[4] Fachbereich Physik, Freie Universität Berlin, Arnimallee 14, D-14195 Berlin-Dahlem, Germany
[5] Department of Physics and Astronomy, Uppsala University, SE-75120 Uppsala, Sweden
[*] Author to whom any correspondence should be addressed.

E-mail: edwin.kukk@utu.fi and puettner@zedat.fu-berlin.de

Keywords: photoemission, vibrational structure, HAXPES, recoil, Doppler broadening

Abstract

Doppler and recoil effects are an integral part of the photoemission process at the high kinetic energies reached in hard x-ray photo-electron spectroscopy (HAXPES) and have a major effect on the observed lineshape, resulting in broadening, energy losses and discrete excitations. These effects can be modeled with a high degree of detail for small systems like diatomic molecules, for larger systems such treatment is often superfluous as the fine spectral features are not observable. We present a united description of the Doppler and recoil effects for arbitrary polyatomic systems and offer an approximate description of the recoil- and Doppler-modified photoemission spectral lineshape as a practical tool in the analysis of HAXPES spectra of core-level photoemission. The approach is tested on the examples of carbon dioxide and pentane molecules. The C and O 1s photoelectron spectra of CO_2 in gas phase were also measured at 2.3 and 7.0 keV photon energy at Synchrotron SOLEIL and the spectra were analyzed using the model description. The limitations and applicability of the approach to adsorbates, interfaces and solids is briefly discussed.

1. Introduction

Electron-spectroscopic measurements of photoemission from atomic core orbitals provide valuable information on the chemical environment of the emitter atom, geometry of the containing compound and its changes upon core ionization. Analysis of the photoelectron spectra provides quantities such as chemical shifts [1], vibrational frequencies, Franck–Condon factors [2] and core-hole lifetimes [3] that are closely linked to fundamental chemical–physical properties. However, a full account of all the components making up the structure of the photoelectron spectra is an essential prerequisite for the accurate extraction of such information.

In the case of core-level photoemission, a particular atom in a molecule, liquid or solid can be associated with the process. Then, as the photoelectron carries away a certain momentum, *recoil* occurs as an integral part of the photoemission process [4–16]. While the influence of recoil on the photoelectron spectrum is usually minimal in low-kinetic-energy spectra measured near the ionization edge, it becomes significant as the kinetic energy increases. New scientific opportunities brought by the advances in techniques and light sources have created an active hard x-ray photo-electron spectroscopy (HAXPES) community [17–23]. In this regime, the recoil effects cannot be ignored.

An atom is never completely at rest and the thermal motion of the emitter atom introduces another inherent feature in photoemission—the Doppler broadening. Translational Doppler broadening in photoemission from atomic or molecular gases is well known [24–26]; more recently, rotational Doppler broadening in molecular photoemission was added to the description [27, 28]. It is worth pointing out a

close relationship between the recoil and Doppler effects in photoemission—both, as seen in the observer's frame of reference, arise from momentum sharing between the emitter and the photoelectron. In Doppler effect, the emitter's existing momentum is added to the photoelectron's; in recoil, the emitter's recoil momentum is removed from it. Both can become prominent, if the emitter atom can acquire a significant individual momentum by recoil and by thermal motion. Here, we combine the recoil and Doppler effects in a complete treatment of all recoil-related features in the photoelectron spectra. In particular, we take into account that in molecules, the Doppler broadening occurs due to the atomic motion in *all* degrees of freedom, not only translational or rotational and, furthermore, that the atomic motion is present even at zero temperature due to the quantum nature of the molecular vibrations.

Molecular photoemission offers a useful testbed for theoretical models of the recoil-related effects and their practical application. Recent opportunities for high-resolution gas-phase electron spectroscopy in the tender x-ray regime (ca 2–10 keV) have advanced our understanding of the recoil effects in diatomics [10, 29]. Recoil effects have also been studied in solids [8, 18, 30, 31] and in some examples of polyatomic molecules such as CH_4 [6] and CF_4 [10, 32]. A general quantum mechanical treatment is available to be extended, in principle, to polyatomic molecules of any complexity [5, 12, 29, 32]. However, the photoelectron spectra of the larger quantum systems are typically highly convoluted and the fine structural details are hidden. Extending a detailed recoil treatment to much larger systems is a time-consuming task with diminishing returns, in particular when the goal is not to investigate recoil-related effects *per se* but rather to adequately account for them in a general analysis of HAXPES spectra of molecules in gas phase, on surface or embedded, or as molecular solids.

Here, we propose a unified model for treating recoil and Doppler effects that ultimately presents the lineshape in the photoelectron spectrum in an approximate but simple analytical form. For brevity, we will refer to it as the *recoil lineshape* and it captures the essential features of the lineshape—energy shifts, broadenings and asymmetry, while removing details from the quantized energy level structure. We apply the recoil lineshape (both the more accurate and the approximate formulations) to specific examples of core-level photoemission from carbon dioxide and pentane in the tender x-ray regime. While in modeling the recoil lineshape can be treated in isolation, in application to measured photoelectron spectra, a number of other contributions to the lineshape must be included as well. The Franck–Condon vibrational excitations, the Lorentzian broadening due to the finite lifetime of the core hole and the instrumental broadening will all be included and combined with the recoil and Doppler contribution when dealing with the experimental spectra.

Carbon dioxide is a particularly interesting test case, where both the detailed and approximate recoil lineshape treatments are practical, the latter at the limits of its intended purpose as a convenient description of recoil-related effects in any polyatomic system. We compare the modeled recoil effects with measurements performed at the GALAXIES beamline of the SOLEIL synchrotron. The comparison is particularly beneficial due to the latest instrumental developments—the introduction of a high-resolution crystal monochromator allowing to reduce the photon bandwidth dramatically and providing a much more stringent test for the recoil lineshape than was possible before.

Lastly, we model the recoil lineshape in a 'proper' polyatomic molecule, pentane, for the C 1s photoemission from its three inequivalent carbon atoms, pointing out some general trends as the molecules grow in size and also condensing the generation of the recoil lineshape into a practical recipe.

2. Modeling recoil lineshape

2.1. Atomic photoemission

When a free atom emits a photoelectron, energy in the amount of

$$E_{\mathrm{em}} = h\nu - E_{\mathrm{b}} \tag{1}$$

becomes available as the kinetic energy in the system of the emitter atom and the photoelectron, where $h\nu$ is the energy of the absorbed photon and E_{b} the binding energy of the emitted electron. The kinetic energy $E_{\mathrm{kin}}^{\mathrm{el}}$ of the photoelectron is smaller than E_{em} due to the recoil of the emitter. If the atom is initially at rest, then from the energy and momentum conservation and by taking into account that the mass of the electron m_e is much smaller than that of the emitter atom m_a, the kinetic energy of the electron $E_{\mathrm{kin}}^{\mathrm{el}}$ and the recoil energy $E_{\mathrm{r}}^{\mathrm{at}}$ of the emitter atom are

$$\begin{aligned} E_{\mathrm{kin}}^{\mathrm{el}} &= E_{\mathrm{em}} - E_{\mathrm{r}}^{\mathrm{at}}, \\ E_{\mathrm{r}}^{\mathrm{at}} &\cong \gamma E_{\mathrm{em}}, \quad \gamma \equiv \frac{m_e}{m_a}. \end{aligned} \tag{2}$$

Since atoms in the gas are in thermal motion, in the observer's frame of reference the photoelectron experiences not only the loss of the momentum due to recoil but also addition of the initial momentum of the emitter. Consequently, the recoil energy E_r^{at} for an a particle at rest becomes the average value $\overline{E}_r^{at}$ for the distribution caused by the Doppler broadening in photoemission from moving emitters, as developed below. We will combine the total change of momentum and the corresponding energy change under the *recoil energy* term:

$$E_r^{at} = \left(\gamma - 2\frac{v_{A,e}}{v_e}\right) E_{em}, \tag{3}$$

where v_e is the velocity of the photoelectron and $v_{A,e}$ is the component of the atomic velocity $\vec{v}_A$ along the photoemission direction $\hat{v}_e$. Equation (3) is the basis of the unified treatment of the recoil and Doppler effect, and next we will develop the distributions of the recoil energy in atomic (E_r^{at}) and molecular (E_r) cases.

According to the Maxwell–Boltzmann distribution,

$$F_{MB}(v_{A,e}) \propto \exp\left(-\frac{1}{2}\frac{m_a v_{A,e}^2}{k_B T}\right), \tag{4}$$

where k_B is the Boltzmann constant and T the temperature. Combining equations (3) and (4), we see that the distribution of the recoil energy follows the Gaussian (normal) distribution:

$$\begin{aligned} F_G^{at}(E_r^{at}) &= \frac{1}{\sigma^{at}}\sqrt{2\pi}\,\exp\left(-\frac{1}{2}\frac{(E_r^{at}-\overline{E}_r^{at})^2}{\sigma^{2,at}}\right), \\ \sigma^{2,at} &= 2\gamma E_{em} k_B T. \end{aligned} \tag{5}$$

We note that the distribution F_G^{at} also gives the *recoil lineshape* in the photoelectron kinetic energy spectrum (equation (3)), incorporating both the recoil shift $\overline{E}_r^{at}$ and the well-known translational Doppler broadening [24], characterized by the variance $\sigma^{2,at}$. The variance can be expressed using the mean kinetic energy of the emitter atoms per one degree of freedom:

$$\sigma^{2,at} = 4\gamma E_{em}\overline{E}_T\,,\ \overline{E}_T = \frac{k_B T}{2}. \tag{6}$$

With the extension to the molecular photoemission in mind, let us obtain $F_G^{at}(E_r)$ by considering the three degrees of motion as independent randomly oriented 'oscillators', each of which has the velocity distribution $F_{MB}(v_{A,n})$ according to the Maxwell–Boltzmann distribution (equation (4)). As these oscillators are not aligned with the photoemission direction, their velocity distributions must be projected onto the photoemission axis $\hat{v}_e$ in order to obtaining the Doppler broadening. For isotropically oriented oscillators, $\overline{v^2}_{A_n,e} = \frac{1}{3}\overline{v^2}_{A_n}$ and the contribution of each oscillator n to the recoil energy distribution can be expressed as

$$\begin{aligned} F_{G,n}^{at}(E_r^{at}) &= \frac{1}{\sigma_n\sqrt{2\pi}}\,\exp\left(-\frac{1}{2}\frac{(E_r^{at}-\overline{E}_{r,n}^{at})^2}{\sigma_n^2}\right), \\ \overline{E}_{r,n}^{at} &= \frac{1}{3}\gamma E_{em}, \quad \sigma_n^2 = \frac{4}{3}\gamma E_{em}\overline{E}_T. \end{aligned} \tag{7}$$

The total recoil energy distribution is a convolution of the contributions by the three independent oscillators:

$$F_G^{at}(E_r^{at}) = F_{G_1}^{at}(E_r^{at}) \circledast F_{G_2}^{at}(E_r^{at}) \circledast F_{G_3}^{at}(E_r^{at}), \tag{8}$$

which has the mean and variance as the sums of the means and variances of the individual distributions:

$$\overline{E}_r^{at} = \gamma E_{em}, \qquad \sigma^{2,at} = 4\gamma E_{em}\overline{E}_T. \tag{9}$$

The result is the same as equations (2) and (6).

2.2. Molecular photoemission at the high-temperature limit

In a gas consisting of N-atomic molecules with mass M, there are $3N$ degrees of freedom: 3 translational, 3(2) rotational (2 for linear molecules) and $3N-6(5)$ vibrational. Let us consider the contributions of all these to the recoil energy distribution as an extension of the atomic case, by associating an independent randomly oriented oscillator, in which the motion of the individual atoms is determined by the normal mode analysis, with each degree of freedom. We limit the treatment to the situation where the photoelectron can be regarded as originating from a particular atom A in the molecule. This is the general assumption of recoil models in high-kinetic-energy photoemission, such as in the HAXPES regime [29, 33].

Then, it is the mass m_A and thermal velocity distribution of the emitter atom, not of the whole molecule, that determines the recoil distribution. According to the equipartition principle, each oscillator contains an average of $\overline{E}_T = k_B T/2$ thermal *kinetic* energy, to which the emitter atom contributes by $f_n\overline{E}_T$, where f_n in the energy fraction of the emitter atom A in oscillator n. Each oscillator then contributes to the total recoil distribution by

$$F_{G,n}(E_r) = \frac{1}{\sigma_n\sqrt{2\pi}}\exp\left(-\frac{1}{2}\frac{(E_r-\overline{E}_{r,n})^2}{\sigma_n^2}\right),$$
$$\overline{E}_{r,n} = \frac{1}{3}\gamma E_{em} f_n, \quad \sigma_n^2 = \frac{4}{3}\gamma E_{em}\overline{E}_T f_n. \tag{10}$$

The recoil energy distributions for molecular degrees of freedom thus differ from the atomic ones (7) by the factors f_n. As in the atomic case, the total recoil distribution is given by the convolution of all $3N$ independent oscillators, from which it is useful to separate the translational, rotational and vibrational contributions that, as well as the total energy distribution, are all given by Gaussian distributions with the following parameters:

$$\overline{E}_{r,tsl} = \gamma E_{em} f_{tsl}, \sigma_{tsl}^2 = 4\gamma E_{em}\overline{E}_T f_{tsl}$$
$$\overline{E}_{r,rot} = \gamma E_{em}\sum_{n\in n_{rot}} f_n, \sigma_{rot}^2 = \frac{4}{3}\gamma E_{em}\overline{E}_T\sum_{n\in n_{rot}} f_n$$
$$\overline{E}_{r,vib} = \gamma E_{em}\sum_{n\in n_{vib}} f_n, \sigma_{vib}^2 = \frac{4}{3}\gamma E_{em}\overline{E}_T\sum_{n\in n_{vib}} f_n \tag{11}$$
$$\overline{E}_r = \overline{E}_{r,tsl} + \overline{E}_{r,rot} + \overline{E}_{r,vib}, \sigma^2 = \sigma_{tsl}^2 + \sigma_{rot}^2 + \sigma_{vib}^2.$$

Here, f_{tsl} represents the sum of f_n over the three translational degrees of freedom that is only dependent of the masses of the emitter and the molecule: $f_{tsl} = m_A/M$. Since the sum of the coefficients f_n (including f_{tsl}) is 3, the total recoil shift and broadening in equation (11) are in fact equal to those for an atomic gas of the emitter atoms A (equation (9)) and there seems to be little benefit in separating the three types of oscillators. However, they do have specific characteristics, especially in vibrational motion.

In order to apply equation (11) to specific cases, the coefficients f_n are needed. We will present a general method for obtaining these, along the example of the O and C 1s photoemission from CO_2, as will be later compared with experiment.

The case of the translational degrees of freedom is the simplest: all atoms have equal velocities and hence $f_{tsl} = m_A/M$, $f_{tsl} = \frac{16}{44}$ ($\frac{12}{44}$) for O (C) 1s photoemission.

In general, each of the $3N$ oscillators represents one normal mode of motion. When the normal-mode vectors are expressed in the coordinate displacement $(x,y,z)_i i = 1,2\ldots,N$ basis, the energy fractions of atom $i = A$ in each mode n are given by

$$f_n = \frac{m_A\left(x_{A,n}^2 + y_{A,n}^2 + z_{A,n}^2\right)}{C},$$
$$C = \sum_{i=1}^{N} m_i\left(x_{i,n}^2 + y_{i,n}^2 + z_{i,n}^2\right), \tag{12}$$

where m_i is the mass of atom i. Returning to our example, the ground-state CO_2 is an inversion-symmetric linear molecule for which the normal mode vectors are easily obtained by hand and are given in table A.1 of the appendix.

While the vibrational modes are quite molecule-specific, some general considerations can be given about the rotational modes. Treating the molecule as a rigid rotor, the kinetic energy of the molecule in each rotational degree of motion is

$$\overline{E}_n = \frac{1}{2}I_n\omega^2 = \overline{E}_T, \quad n\in n_{rot},$$

where I_n in the moment of inertia of the molecule for the given rotational axis in mode n. The kinetic energy of the emitter atom A at the distance R_A from the rotational axis and its energy fraction coefficient are

$$E_{A,n} = \frac{1}{2}m_A R_A^2\omega^2, \qquad f_n = \frac{m_A R_A^2}{I_n}, \quad n\in n_{rot}. \tag{13}$$

In diatomics and linear polyatomics, the convolution is over two degenerate rotational degrees of freedom and we obtain from equations (13) and (11) and using $\overline{E}_T = k_B T/2$, that

$$\sigma_{rot}^2 = \frac{4}{3}\frac{E_{em} m_e R_A^2 k_B T}{I}, \tag{14}$$

which is the formula for the *rotational Doppler broadening* in molecular photoemission, as presented by Thomas *et al* after angular averaging over isotropic photoemission in the molecular frame [34] and developed theoretically by Sun *et al* [27]. (Here, we do not account for the possible changes in the moment of inertia upon core ionization).

2.3. Quantum effects in the recoil from vibrational normal modes

The above results were obtained, neglecting the quantization of the energy levels in all $3N$ oscillators. While this is a very good approximation for the translational and rotational degrees of freedom, for vibrations it is suitable only at very high temperatures. Next we consider the quantization effects on the recoil energy distribution in one vibrational oscillator n, first at $T = 0$ and then at any temperature, using the simplest, harmonic oscillator linear coupling model.

The quantum mechanical treatment of how the photoelectron recoil populates the vibrational energy levels has been developed to a high degree of accuracy for diatomic molecules, and has also been extended to polyatomics. Briefly, the recoil transition intensities between the vibrational levels are obtained as the Franck–Condon factors—squares of the overlap integrals of the initial and final state vibrational wavefunctions—in momentum space [6]. Within the harmonic oscillator linear coupling model, and for the transitions from the ground vibrational level, it is well known that the Franck–Condon factors for recoil excitations $\nu_i = 0 \rightarrow \nu_f$ are conveniently given by Poisson distribution:

$$FC_{0\rightarrow\nu_f} = \frac{S_n^{\nu_f}\, \mathrm{e}^{-S_n}}{\nu_f!}, \quad S_n \equiv \frac{\overline{E}_{\mathrm{r},n}}{\hbar\omega_n}, \tag{15}$$

where the Poisson parameters S_n are the ratios of the average recoil energy deposited into the nth oscillator and its vibrational quantum. The average recoil energy is given, as in the classical model (equation (10)), by $\overline{E}_{\mathrm{r},n} = \frac{1}{3} f_n \gamma E_{\mathrm{em}}$. (Note that the factors f_n are the same as in the quantum-mechanical model [32].) The vibrational transition intensities can be mapped onto the continuous recoil energy distribution as delta-functions:

$$F_{\mathrm{P},n}(E_\mathrm{r}) = \sum_{\nu_f} FC_{\nu_i\rightarrow\nu_f}\, \delta(E_\mathrm{r} - (\nu_f - \nu_i)\hbar\omega_n). \tag{16}$$

Keeping with the aim of providing an overall characterization of the recoil lineshape, we will not concentrate on the individual recoil-excited transitions but rather on characterizing the resultant vibrational envelope as a distribution function, by its first (mean recoil energy), second (variance) and third (skewness) statistical moments. The skewness μ is a measure of asymmetry of the distribution and we use its normalized, dimensionless definition. The Poisson distribution has the first moments (mean, variance and skewness),

$$\begin{aligned} \overline{E}_{\mathrm{r},n} &= S_n \hbar\omega_n, \\ \sigma_n^2 &= S_n \hbar\omega_n^2, \\ \mu_n &= \sqrt{\frac{1}{S_n}}. \end{aligned} \tag{17}$$

The Poisson-distributed vibrational envelope is thus asymmetric toward the $E_{\mathrm{r},n} > \overline{E}_{\mathrm{r},n}$ side but approaches the symmetric Gaussian shape when the vibrational quantum is much less than the recoil energy ($\mu_n \rightarrow 0$). Taking into account that the average kinetic energy in a quantum oscillator in zero-point motion is $\overline{E}_{\hbar\omega,n} = \frac{1}{4}\hbar\omega_n$, the variance can be expressed also as

$$\sigma_n^2 = \frac{4}{3}\gamma E_{\mathrm{em}} \overline{E}_{\hbar\omega,n} f_n. \tag{18}$$

This expression has a close analogy with σ_n^2 in equation (10), replacing the thermal energy in the oscillator with the zero-point kinetic energy. This leads to a physical interpretation of the origin of the recoil-induced vibrational progression: *the emitters as quantum oscillators have zero-point vibrational motion that causes Doppler broadening in photoemission even at $T = 0$ K. That broadening itself is quantized by the vibrational level structure of the oscillator, and appears as the recoil-induced vibrational excitations in the photoelectron spectrum.* In terms of the recoil lineshape in photoemission, the main effect of the quantization is the additional broadening due to the zero-point kinetic energy. In addition, the lineshape becomes asymmetric, as that additional contribution is characterized by Poisson, not Gaussian distribution.

The combined contribution of the vibrational recoil envelopes related to the zero-point motion, over all n_{vib} degrees of freedom, is given by the combination bands in the quantum mechanical treatment. In terms of the recoil lineshapes $F_\mathrm{P}(E_n)$ in our treatment, the combined contribution is given by their convolution,

with the first moments given (in analogy with equation (11)) by

$$\begin{aligned}\overline{E}_{\mathrm{r,vib}} &= \sum_{n\in n_{\mathrm{vib}}} S\hbar\omega_n = \frac{1}{3}\gamma E_{\mathrm{em}} \sum_{n\in n_{\mathrm{vib}}} f_n,\\ \sigma^2_{\mathrm{vib}} &= \sum_{n\in n_{\mathrm{vib}}} S\hbar\omega_n^2 = \frac{1}{3}\gamma E_{\mathrm{em}} \sum_{n\in n_{\mathrm{vib}}} f_n\hbar\omega_n,\\ \mu_{\mathrm{vib}} &= \frac{1}{\sigma^{3/2}_{\mathrm{vib}}} \sum_{n\in n_{\mathrm{vib}}} \sigma_n^{3/2}\sqrt{\frac{1}{S_n}}.\end{aligned} \tag{19}$$

The quantized vibrational oscillators also contain thermal energy, manifested as population of higher initial-state levels $\nu_i > 0$. However, the average thermal kinetic energy is not $\frac{1}{2}k_{\mathrm{B}}T$, but is reduced due to quantization. According to [35],

$$\overline{E}_{T,n} = \frac{1}{2}\frac{\hbar\omega_n}{\mathrm{e}^{\frac{\hbar\omega_n}{k_{\mathrm{B}}T}} - 1}. \tag{20}$$

In a detailed quantum-mechanical treatment the recoil vibrational envelope at $T > 0$ contains hot bands, with transition intensities given by the Franck–Condon factors $FC_{\nu_i>0\to\nu_f}$. These are, however, more difficult to calculate than $FC_{0\to\nu_f}$, since for $\nu > 0$ there is no simple counterpart for the Poisson model (equation (15)). Also, at the typical emitter gas temperatures $T \lesssim 300$ K, the hot-band contribution to the recoil energy distribution is minor compared to the translational, rotational and vibrational zero-point Doppler broadenings. Therefore, we add the hot-band contribution to each vibrational profile as Gaussian broadening according to equation (10), but taking into account that the thermal energy is reduced in vibrational oscillators (equation (20)). Each vibrational oscillator contributes a variance

$$\sigma^2_{T,n} = \frac{4}{3}\gamma E_{\mathrm{em}}\overline{E}_{T,n} f_n, \tag{21}$$

and obtain the total hot-band broadening as

$$\sigma^2_T = \sum_{n\in n_{\mathrm{vib}}} \sigma^2_{T,n}.$$

2.4. Combining classical and quantum oscillators

We now have all the individual distributions of the $3N$ oscillators, their means, variances and skewnesses. In addition to the Poisson distributions of the zero-point vibrational envelopes, there are a number of Gaussian contributions—the translational and rotational recoil shifts and Doppler broadenings as well as the vibrational hot-band broadening (the vibrational recoil shift is already included in the vibrational Poisson distributions). The total recoil lineshape is a convolution of all these distributions, and we first combine the symmetric Gaussian and the skewed Poisson distributions into $F_{\mathrm{G}}(E_{\mathrm{r}})$ and $F_{\mathrm{P}}(E_{\mathrm{r}})$, respectively:

$$\begin{aligned}F_{\mathrm{tot}}(E_{\mathrm{r}}) &= F_{\mathrm{P}}(E_{\mathrm{r}}) \circledast F_{\mathrm{G}}(E_{\mathrm{r}}),\\ \overline{E}_{\mathrm{r,P}} &= \overline{E}_{\mathrm{r,vib}}, \qquad \sigma^2_{\mathrm{P}} = \sigma^2_{\mathrm{vib}};\ \ \mu_{\mathrm{P}} = \mu_{\mathrm{vib}},\\ \overline{E}_{\mathrm{r,G}} &= \overline{E}_{\mathrm{r,tsl}} + \overline{E}_{\mathrm{r,rot}}, \qquad \sigma^2_{\mathrm{G}} = \sigma^2_{\mathrm{tsl}} + \sigma^2_{\mathrm{rot}} + \sigma^2_T.\end{aligned} \tag{22}$$

The final molecular recoil lineshape $F_{\mathrm{tot}}(E_{\mathrm{r}})$ has no general closed-form expression, but can be characterized by its mean, variance and skewness:

$$\begin{aligned}\overline{E}_{\mathrm{r,tot}} &= \overline{E}_{\mathrm{r,P}} + \overline{E}_{\mathrm{r,G}} = \gamma E_{\mathrm{em}}, \qquad \sigma^2_{\mathrm{tot}} = \sigma^2_{\mathrm{P}} + \sigma^2_{\mathrm{G}},\\ \mu_{\mathrm{tot}} &\approx \left(\frac{\sigma_{\mathrm{vib}}}{\sigma_{\mathrm{tot}}}\right)^{\frac{3}{2}} \mu_{\mathrm{vib}}.\end{aligned} \tag{23}$$

In all the convolutions, the individual means and variances are simply added, as is the case for the Gaussian and Poisson distributions. The skewness of their combined distribution has, to our knowledge, no exact expression; it is carried from the Poisson distribution with the appropriate weight by which he Poisson distribution contributes to the combined one.

As an example, table 1 summarizes the recoil shifts, broadenings and asymmetry in the recoil lineshape for the O and C 1s core ionization in CO_2 by 7 keV photons (as in the experimental spectra presented later). By giving a comparison of the classical and quantum vibrational oscillator model predictions, the contribution of the zero-point vibrational motion and the asymmetry caused by the quantization of the

Table 1. Recoil energy shifts, broadenings (in meV) and asymmetry (as skewness μ) in the O and C 1s photoemission from CO_2 molecule by 7 keV photons at $T = 300$ K. The values are listed for translational (tsl), rotational (rot) and vibrational (vib) degrees of freedom, the latter subdivided to the zero-point ($\text{vib}_{\hbar\omega}$) and thermal contributions (vib_T).

Mode	O 1s			C 1s		
	$\overline{E}_r$	σ	μ	$\overline{E}_r$	σ	μ
			Classical			
tsl	80.4	64.5		83.5	65.7	
rot	73.7	61.7		0.0	0.0	
vib	67.0	58.9	0.0	222.8	107.3	0.0
tot	221.2	106.9	0.0	306.3	125.8	0.0
			Quantum			
tsl	80.4	64.5		83.5	65.7	
rot	73.7	61.7		0.0	0.0	
vib_T	0.0	12.7	0.0	0.0	32.2	0.0
$\text{vib}_{\hbar\omega}$	67.0	103.3	1.807	222.8	184.2	1.170
tot	221.2	137.1	0.773	306.3	198.2	0.939

vibrational oscillators is demonstrated. In O 1s emission, for example, thermal vibrational motion in non-quantized oscillators would contribute about 60 meV to the recoil broadening (σ) at room temperature, while in quantum oscillators it is reduced to 13 meV, since the oscillators' capacity to receive thermal energy is diminished. On the other hand, the temperature-independent purely quantum zero-point motion now contributes the largest broadening, 103 meV, which is also the source of the asymmetry (μ) of the total lineshape.

2.5. Approximate recoil lineshape

In practical applications such as curve fitting, it is useful to employ an analytical lineshape for the recoil effects, instead of the numerical convoluted distribution $F_{\text{tot}}(E_r)$. Also, in the case of polyatomic molecules with many vibrational normal modes that are recoil-active, the individual vibrational peaks of $F_P(E_r)$ will be indistinguishable after the convolution by $F_G(E_r)$ and by the lifetime Lorentzian broadening of the core-hole state. Here, we demonstrate a convenient approximation that correctly represents the main characteristics—the recoil shift, broadening and the asymmetry of the quantized vibrational excitations—using a three-parameter continuous distribution function. The *translated gamma* distribution is often used in statistics to represent skewed distributions:

$$F_\Gamma(E_r) = \frac{(E_r + \epsilon)^{k-1}}{\Gamma(k)\theta^k} \exp\left(-\frac{E_r + \epsilon}{\theta}\right), \tag{24}$$

where $\Gamma(k)$ is the gamma-function. The distribution $F_\Gamma(E_r)$ matches the first three moments of the recoil lineshape $F_{\text{tot}}(E_r)$, when

$$k = \frac{4}{\mu_{\text{tot}}^2}, \qquad \theta = \frac{1}{2}\mu_{\text{tot}}\sigma_{\text{tot}}, \qquad \epsilon = \frac{2\sigma_{\text{tot}}}{\mu_{\text{tot}}} - \overline{E}_{r,\text{tot}}. \tag{25}$$

Below, the use of both the approximate shape and the numerical convolution (equation (22)) is illustrated on the example of a single vibrational oscillator corresponding to the bending vibrations of CO_2, with $\hbar\omega = 83$ meV. The recoil energy distributions in figure 1 were generated for the C 1s photoemission at the ionizing photon energy of 7 keV. The distributions also contain the energy shift and broadening from the translational degrees of freedom (there is no rotational recoil). The δ-function distribution of the Franck–Condon intensities for the transitions from the $\nu_i = 0$ level only is shown by vertical bar spectra, shifted by the translational recoil of 83.5 meV. The Franck–Condon intensities including the hot band (from thermally populated $\nu_i > 0$) are marked by '–'.

In the top panel, generated for the LN2 temperature, the modulation by the individual vibrational peaks is visible in $F_{\text{tot}}(E_r)$ as the thermal broadening is small. The approximate shape $F_\Gamma(E_r)$, however, represents the overall envelope quite well, especially when taking into account that in the actual photoelectron spectrum a number of other broadenings will be present. The bottom panel (b) shows the same example, but now generated for the room temperature of 300 K, at which the larger Gaussian component washes out the details of the vibrational structure and the approximate lineshape becomes indistinguishable from the accurate one.

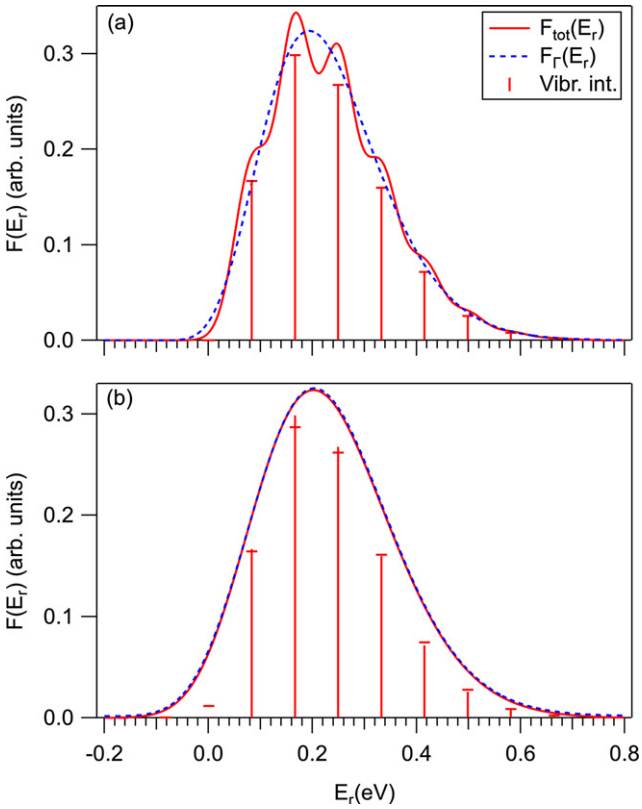

Figure 1. Recoil energy distributions in the bending-mode oscillator of CO_2, including thermal Doppler broadening in this vibrational mode and from the translational modes. Panel (a): $T = 77$ K, (b): $T = 300$ K. Vertical bars are the vibrational excitations from the $\nu_i = 0$ level and the horizontal markers show the excitations modified by the hot-band contribution. Solid red lines show the recoil distributions by numerical integration (equation (22)) and the dashed blue lines the approximate shape (equation (24)).

3. Recoil lineshape applied to polyatomic molecules

3.1. Carbon dioxide

3.1.1. Modeling

Figure 2 shows the total recoil lineshapes $F_{tot}(E_r)$ (equation (22)) and their approximations by $F_\Gamma(E_r)$ (equation (24)) for the O 1s (panels (a) and (b)) and C 1s (panels (c) and (d)) photoemission from gas-phase CO_2 molecules. The energy partitioning factors are from table A.1 (appendix) and the ground-state vibrational frequencies (83 meV for bending, 165 meV for symmetric and 291 meV for asymmetric stretching) were used. The lineshapes were calculated at the temperature of 300 K for two photon energies, 2.3 keV (panels (a) and (c)) and 7 keV (panels(b) and (d)). The figure also shows convolutions with lifetime Lorentzian broadening of 165 meV (FWHM) for the O 1s [36] and 99 meV for the C 1s core hole state [3]. The vibrational transition probabilities $F_P(E_r)$ (for $T = 0$ K) are shown by the vertical bars.

The O 1s spectrum at 2.3 keV (a) has weak recoil excitations in all vibrational modes. The total vibrational envelope is strongly asymmetric, with $\mu = 1.48$, and in this regime the approximation by the gamma distribution F_Γ has significant deviations from the true convolution F_{tot}. However, when the lifetime broadening, as an inherent component in photoelectron spectra, is added, the F_Γ description matches F_{tot} (dashed lines in figure 2(a)) very well. At the higher photon energy of 7 keV, there are stronger vibrational excitations as well as a large Gaussian component in the C 1s recoil lineshape. The total recoil profile now has the asymmetry $\mu = 0.77$ and the approximate lineshape F_Γ is a much better fit to F_{tot} already before adding the lifetime broadening. Again, after adding the lifetime broadening the differences between F_Γ and F_{tot} all but disappear.

The C 1s spectra (b) and (d) exhibit similar characteristics, although in this case the Gaussian contribution is less since there is no rotational recoil (and consequently no rotational Doppler broadening). On the other hand, a large fraction of the recoil energy goes into the bending vibrational oscillators (see table A.1). The asymmetry of the profile is reduced from $\mu = 1.72$ at 2.3 keV to $\mu = 0.94$ at 7 keV.

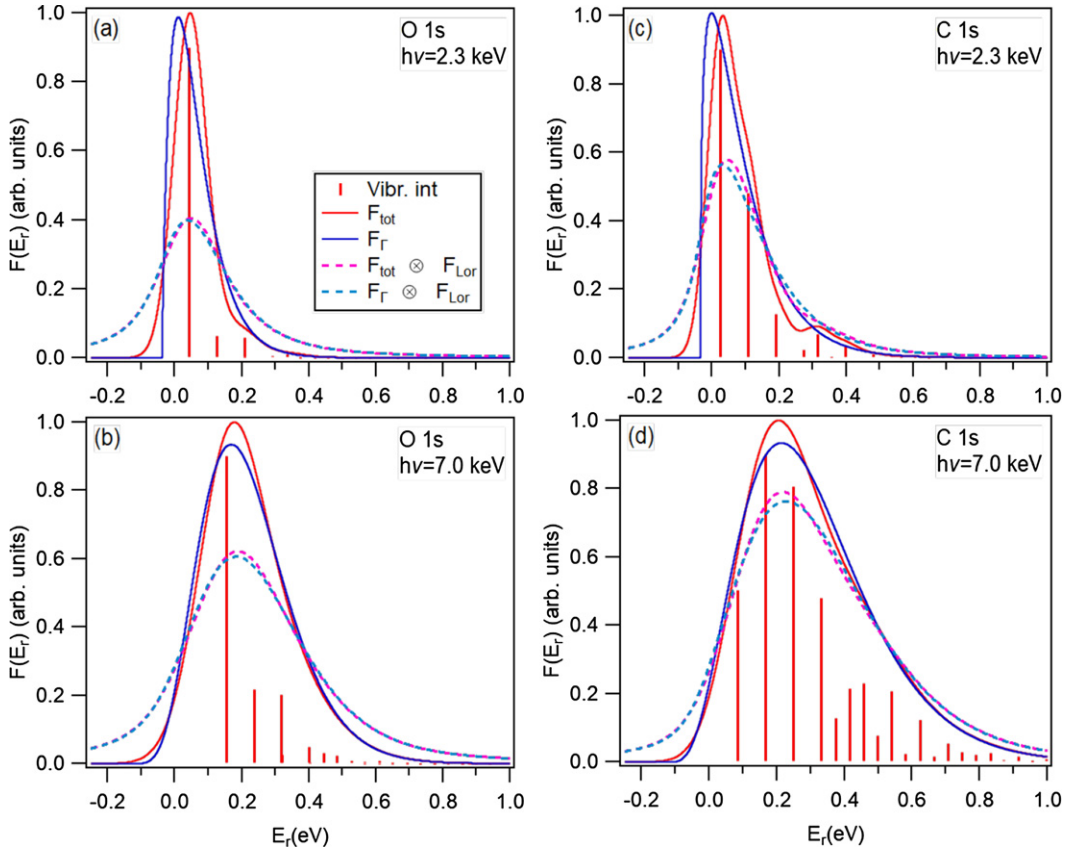

Figure 2. Modeled recoil energy distributions in O 1s (a) and (b) and C 1s (c) and (d) photoemission from CO_2 at the ionizing photon energy of 2.3 keV ((a) and (c)) and 7.0 keV ((b) and (d)), at 300 K. The solid red lines were obtained by numerical convolution, blue lines but the approximate translated gamma distribution and the dashed lines of corresponding color are further convoluted by the lifetime Lorentzian.

3.1.2. Experimental details

The C and O 1s photoelectron spectra of CO_2 were measured at the SOLEIL Synchrotron, France, on the GALAXIES beamline equipped with an end station dedicated to hard and tender x-ray photoelectron spectroscopy [17, 37]. Linearly polarized light is provided by a U20 undulator and monochromatized by a Si(111) double crystal monochromator. A four-bounce high resolution monochromator (HRM) can be inserted in the beam to further narrow down the incident energy bandwidth specially at high energy. At some energies it was necessary to reduce the photon flux at the sample in order to avoid nonlinearity effects associated with the readout of the CCD detector of the Scienta spectrometer.

The CO_2 sample and the calibration gas argon were introduced into a differentially pumped gas cell. The photoelectron spectra were recorded by a large acceptance angle EW4000 Scienta hemispherical analyser, optimized for high kinetic energy measurements. The spectrometer was mounted with the lens axis colinear with the polarization vector of the x-rays. In this experiment, the spectrometer was operated at 100 eV pass energy and with the entrance slit of 0.3 mm (curved). Argon was used to determine the instrument function at the two used photon energies, 2.3 keV and 7.0 keV, as described in [29]. The instrument function thus obtained consisted of a single Gaussian with FWHM of 165 meV at 7.0 keV and a Gaussian doublet with FWHMs of 183 meV, separation of 166 meV and the intensity ratio of 0.251 at 2.3 keV. The instrument function at 7 keV became narrower than at the lower energy using the HRM with asymmetric Si(110) reflection [38]. At 2.3 keV, photon flux was reduced using Al foil filters in order to avoid detector saturation.

3.1.3. Comparison with experiment

The modeled recoil lineshapes (in the kinetic energy scale as by equation (3)) can now be tested against the experimental spectra. Figure 3 shows least-squares curve fitting results for both the oxygen (panels (a) and (b)) and carbon ((c) and (d)) 1s photoelectron spectra at the photon energies of 2.3 keV ((a) and (c)) and 7 keV ((b) and (d)), using the recoil lineshapes of figure 2 with their parameters listed in table 2.

The actual molecular photoemission spectra exhibit, as a rule, vibrational excitations due to another mechanism—the Franck–Condon excitations arising when the potential energy surface of the molecule

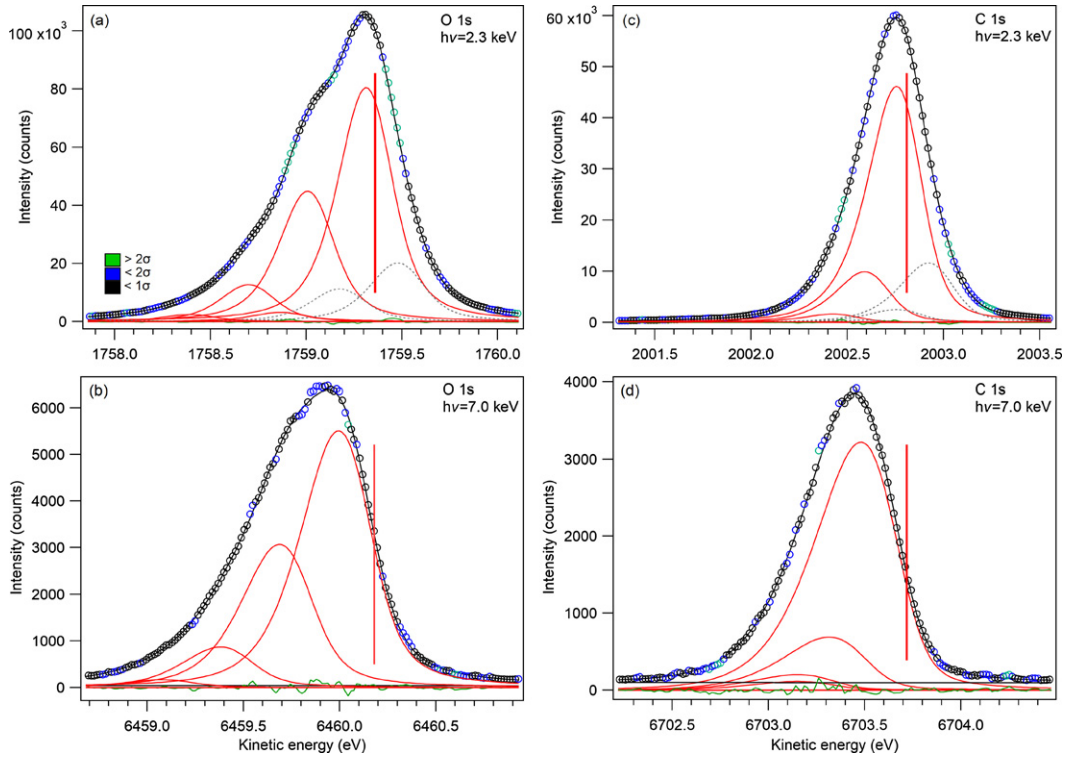

Figure 3. Least-squares curve fitting results of core-level photoelectron spectra of CO_2. The measured spectra (○) are color-coded according to the datapoints' deviation from the fit result given by the black curve. Red curves are the individual recoil lineshapes representing the Franck–Condon series and the green lines are the fitting residuals. Dotted gray curves in (a) and (c) correspond to the contribution from the second component of the instrumental function. Vertical bars denote the nominal kinetic energy.

changes upon ionization. These excitations combine with the recoil excitations in the photoelectron spectrum. Contrary to the recoil-related effects, they are in a good approximation independent of the kinetic energy of the photoelectrons (unless very close to the ionization threshold). Both the Franck–Condon and recoil excitations can be accounted for together using the generalized Franck–Condon factors [5, 29]. However, these two types of excitations are not significantly coupled and are treated independently here—each Franck–Condon excitation peak is represented by one recoil lineshape in the fit. Assuming that the Franck–Condon excitation intensities are independent of photon energy, common peak intensity ratios are imposed to the 2.3 keV and 7 keV spectra.

In least-squares fitting, various scenarios can be applied. The Franck–Condon intensities, peak spacings and the lifetime widths can be taken from the reference data, or left as free parameters. Also, the parameters describing the recoil profiles can be allowed to vary or be fixed according to the model. Here, we present one such scenario, testing the suitability of the approximate recoil lineshape for the experimental high-resolution HAXPES molecular photoelectron spectra. The data from the near-threshold spectra [36, 39, 40] have experimental uncertainties, potentially carrying over significant discrepancies to our fit. Therefore, the Lorentzian lifetime widths of the O and C 1s peaks were used as adjustable parameters, but set equal in both the 2.3 keV and 7 keV spectra. Similarly, the intensity ratios in the Franck–Condon excitation series' (asymmetric stretching in the O 1s and symmetric stretching in the C 1s spectra) were adjustable, but kept equal at the two ionization energies. The vibrational spacings were taken as fixed from [3, 36]. The recoil profiles were convoluted with a free-width Lorentzian lifetime broadening and a Gaussian representing the instrumental contribution.

The lower-energy O 1s spectrum (a) is the most demanding to describe well, both because of its excellent statistics and since the approximate recoil lineshape at this relatively low kinetic energy is near the limit of its suitability. Also, as observed previously and described in subsection 3.1.2, the monochromator's contribution to instrument function is ill-represented by a single Gaussian at 2.3 keV, requiring a Gaussian doublet for a better description, obtained from the fit of Ar 2*p* calibration spectra. That second 'ghost' profile is shown by the gray dotted lines in figures 3(a) and (c), with a shift and relative intensity fixed to the values from the calibration spectrum. The spectra (a) and (b) were fitted together, therefore improving the accuracy of the free parameters. The same fitting procedure was followed for the two C 1s spectra (c) and (d). In fitting both sets of spectra, the total number of free parameters was five plus the intensity ratios of

Table 2. Least-squares fitting parameters and results for the O and C 1s photoelectron spectra of CO_2. All energy values are in meV. 'Instr' refers to the instrumental resolution (FWHM) as determined from the CO_2 and the calibrant Ar spectra.

	O 1s	C 1s
Γ_{lifetime}	167(1)	95.0(6)
$\hbar\omega_{\text{sym.str.}}$ [a]		165.5
$\hbar\omega_{\text{asym.str.}}$ [a]	307	
$I_{\nu=1}/I_{\nu=0}$	0.558(10)	0.230(15)
$I_{\nu=2}/I_{\nu=0}$	0.158(4)	0.033(4)
$I_{\nu=3}/I_{\nu=0}$	0.030(1)	—
$I_{\nu=4}/I_{\nu=0}$	0.005(1)	—
	hν= 2.3 keV	
$\overline{E}_r$ [a]	60.0	91.4
σ_{tot} [a]	71.4	108
μ_{tot} [a]	1.48	1.72
Instr(CO_2)	186(2)	189(2)
Instr(Ar) [b]	183	183
	hν= 7.0 keV	
$\overline{E}_r$ [a]	221	306
σ_{tot} [a]	137	198
μ_{tot} [a]	0.77	0.94
Instr(CO_2)	146(6)	155(4)
Instr(Ar) [b]	165	165

[a] Fixed-value parameter.
[b] Value given for comparison, not used in the fit.

Table 3. Literature values for core-hole lifetime widths and vibrational branching ratios in the O and C 1s photoelectron spectra. Energies are in meV.

	O 1s [36]	C 1s [39]	O 1s [40]	C 1s [40]
Γ_{lifetime}	165	99	163	95
$I_{\nu=1}/I_{\nu=0}$	0.552	0.241	0.553	0.262
$I_{\nu=2}/I_{\nu=0}$	0.155	0.016	0.151	0.028
$I_{\nu=3}/I_{\nu=0}$	0.034	—	0.028	

the Franck–Condon excitations. The overall agreement of the fit with data is excellent, with some regions of minor discrepancies.

The values of the Franck–Condon intensities and lifetime widths are listed in table 2 and a comparison with the values from literature (table 3) shows a very good agreement overall. The purpose of the present analysis is not, of course, to determine these values, but rather to confirm that the recoil effects are properly accounted for. The recoil lineshape includes all Doppler broadenings (including the zero-point vibrational ones) of the photoelectron spectrum at the given temperature, and all recoil energy losses. The fitted peak positions, corresponding to the nominal photoemission kinetic energy (equation (3)) are shown as vertical lines. With a very accurate experimental energy-scale calibration, these positions would be a good test of the recoil model; if such calibration is not available (as in the present spectra), the recoil fit itself can be used for accurate calibration of the energy scale.

A comparison with the instrumental function from the Ar 2*p* calibration spectra and from the CO_2 spectra is another indicator for the suitability of the recoil lineshape, where the discrepancies would reveal unaccounted contributions. As seen from table 2, that is not the case—in general the obtained instrument function is very close to what was obtained from the Ar calibration. At 7 keV the instrumental broadening is slightly less than expected. However, it is the smallest contribution to the total linewidth (in addition to the lifetime broadening of 167 meV and the recoil profile's FWHM of 323 meV), making the determination of its width less accurate. Also, since the given statistical error cannot account for the energy-scale drift correction (applied to a long series of individual spectra measured overnight), the difference is likely not significant.

In conclusion, in the tender x-ray regime the approximate recoil lineshape is able to represent very well the spectral features of the smallest polyatomic molecules. We also used symmetric Voigt lineshapes for fitting the Franck–Condon excitations, which gives a clearly inferior fit to the data. The difference might not be clear for spectra with lower statistics, but, and more importantly, the improper lineshape

significantly distorts the results such as the intensity ratios or line widths. For example, a decomposition of the C 1s spectra (c) and (d) of figure 3 using Voigt profiles but otherwise the same fitting scenario gives the intensity ratio of the Franck–Condon peaks as $I_{\nu=1}/I_{\nu=0} = 0.41$ and $I_{\nu=2}/I_{\nu=0} = 0.132$, about two and four times higher, correspondingly, than the literature values [39].

3.2. Application of the recoil lineshape model to larger molecules—summary of the procedure on the example of pentane

Triatomic molecules such as CO_2 provide a good testing ground for approximate recoil lineshape models and already the added simplicity is very useful in, e.g., curve fitting analysis. However, the approach is primarily intended for larger polyatomics and is indeed easily scaled to much larger molecules. Here, we present the recoil lineshapes in the HAXPES regime using the example of pentane C_5H_{15}, an approximately linear molecule with three chemically inequivalent carbons in the chain. The purpose here is not a comparison with experimental data or further validation of the model, but rather to present an 'illustrated recipe' for obtaining recoil lineshapes for polyatomics of essentially arbitrary size. The concrete example also gives insights into the sensitivity of recoil lineshape on the specific location of the photoemission site in the molecule. Application of the recoil lineshape mode is summarized below:

(i) The normal mode analysis was done using the GAMESS quantum chemistry package [41], providing the normal-mode vectors as coordinate displacements and their frequencies.

(ii) The energy division factors f_n were calculated for all 51 oscillators according to equation (12).

(iii) In an iteration over all the vibrational oscillators, the Poisson parameters S_n (equation (15)) were calculated and the combined vibrational recoil profile's mean energy, variance and skewness obtained (equation (19)). Also, the total thermal kinetic energy (equation (21)) in the vibrational oscillators was calculated.

(iv) The mean recoil energy and broadening (variance) (equation (11)) in the translational and rotational oscillators was obtained, to which the vibrational thermal broadening was added (equation (23)).

(v) The parameters (equation (25)) for the approximate F_Γ lineshapes were calculated and the lineshapes shown in figure 4 generated.

For comparison, in a more detailed but more elaborate representation of the recoil lineshape, the steps (iii) and (v) were replaced by:

(iii) In a summation over all the vibrational oscillators, the Poisson parameters S_n were calculated (equation (15)) and the individual Poisson intensity distributions mapped onto the continuous distribution as delta-functions (equation (16)). The combined Poisson distribution (shown in figure 4) as vertical bars) was obtained by cumulative convolutions of the individual distributions.

(iv) As above.

(v) The final recoil lineshape F_{tot} (equation (22)) was obtained by numerical convolution of the Gaussian and convoluted Poisson components.

Note that although figure 4 accounts for all recoil, Doppler and core-hole lifetime effects in the lineshape, the Franck–Condon excitations due to the change of the potential energy surface are not included. In actual photoelectron spectra, as was the case for CO_2 in figure 3, each Franck–Condon transition would be represented by a distribution given in figure 4.

Let us explore the general trends in the recoil lineshape as the molecular size increases. As seen from figure 4(a), even though the total recoil lineshape F_{tot} is a convolution from 51 oscillators, it retains some structural features and a strong asymmetry that is pronounced even after the convolution with the Lorentzian lifetime broadening. The main reason for the strong asymmetry is that the fraction of the vibrational oscillators increases with the size of the molecule ($\frac{1}{6}$ in diatomics, $\frac{4}{9}$ in CO_2 and $\frac{45}{51}$ in pentane) and the zero-point vibrational Doppler broadening becomes the defining factor in the recoil lineshape. The translational and rotational oscillators in the remaining fraction also receive less recoil energy in larger molecules and thus contribute less of the Gaussian component to the recoil lineshape—simply put, since the thermal velocities are smaller for larger molecules. What is the effect of having a large number of individual vibrational oscillators creating the asymmetric recoil lineshape? If, assuming for simplicity that they all have the same vibrational spacing, then distributing the recoil among many oscillators in a polyatomic would not change the eventual convoluted Poisson lineshape at all (since in convolution the Poisson parameters are added again a simple sum). However, large molecules contain many low-frequency normal modes, which reduces the asymmetry. Thus, we have two opposing trends with the increasing size of the molecule—a more dominant (asymmetric) contribution of vibrational oscillators, and the reduction of the effects of quantization (less asymmetry) in the low-frequency modes. In the example of pentane central carbon C3, the asymmetry (skewness μ) of the lineshape is 1.03, and for the C1 (terminal) and C2 carbons, it is 1.28 and 1.04, respectively. For comparison, $\mu = 0.94$ in the C 1s photoemission from CO_2 (table 2) at $h\nu = 7$ keV, and 0.87 from CO, so the lineshape has become notably more asymmetric.

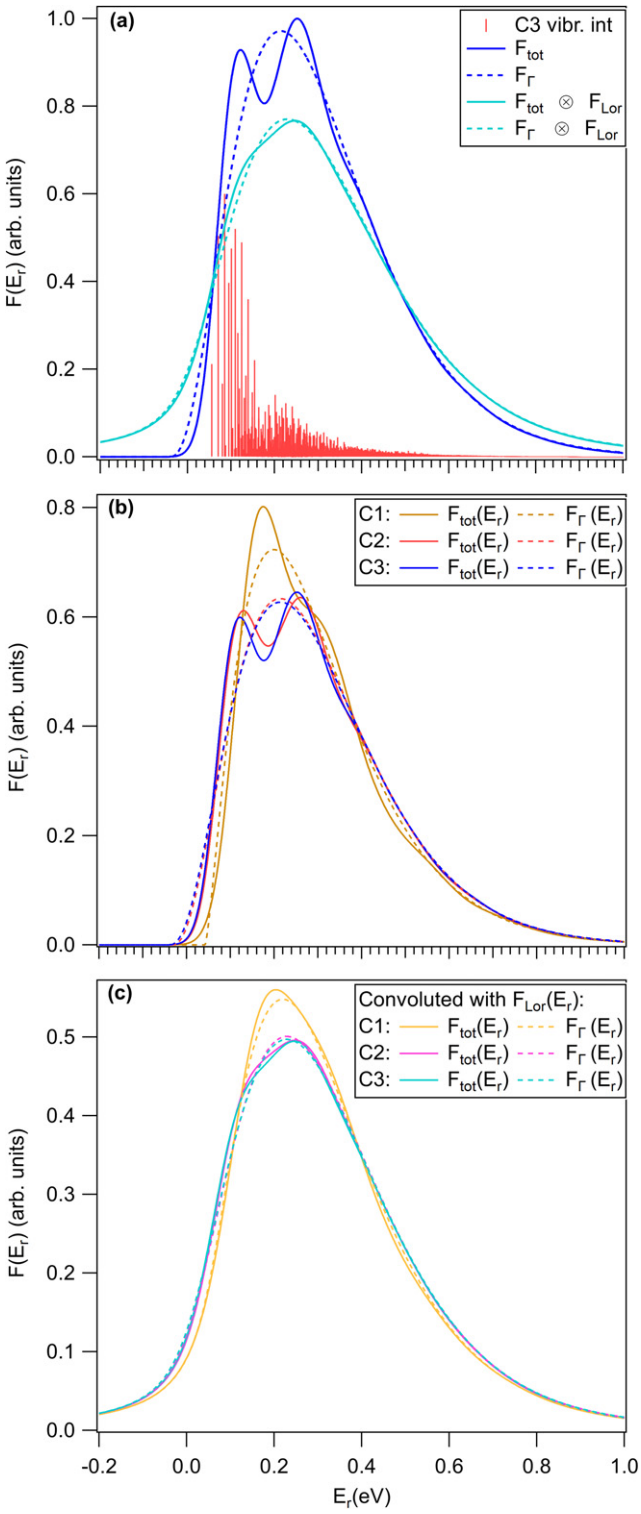

Figure 4. Modeled recoil energy distributions of pentane in C 1s photoemission by 7 keV photons at the liquid nitrogen temperature of 77 K. Panel (a): blue lines show the recoil distribution of the central carbon C3 by the exact (solid curve) and approximate (dotted curve) model representation. The corresponding cyan-colored solid and dotted lines show the shapes after a convolution with Lorentzian of 100 meV FWHM. Panel (b): comparison of the recoil energy distributions of the three chemically inequivalent carbons C1–C3, with the solid lines showing the exact and dotted lines the approximate shape. Panel (c): same as panel (b), but after convoluting with the Lorentzian of 100 meV FWHM.

The variations in the asymmetry and lineshape between C1–C3 are shown in panel (b) of figure 4 and it provides, in principle, a link to the geometry of the emission site. In the given example, the differences would be too small after the lifetime broadening (panel (c)) and Franck–Condon excitations are added. However, they could become more pronounced in an aligned sample (such as adsorbates) versus the isotropically oriented sample of the simulation.

4. Limitations and extensions of the recoil lineshape model

In our combined treatment of recoil and Doppler contributions to the electron energy distributions in molecular photoemission, the molecular normal modes were modeled as *independent* one-dimensional oscillators, randomly oriented in space. This leads to the main limitation, namely neglecting the possible couplings of various normal modes. One mechanism of such a coupling—the Coriolis coupling—was investigated by Thomas *et al* for diatomic molecules. It arises, when the equilibrium bond length changes significantly upon core ionization, changing the moment of inertia of the molecule. If, as is often the case in core-ionization [3], the bond shortens, then as a consequence of angular momentum conservation some of the recoil energy is then diverted from the vibrational to rotational degrees of freedom, changing the energy partitioning $f_{\mathrm{vib}}/f_{\mathrm{rot}}$ from $\frac{1}{2}$ to a lower value [10, 14]. Such couplings, if significant, can be accommodated in the present model by appropriate corrections to the energy fractions f_n of the normal modes.

Let us consider the impact of the Coriolis coupling in the case of CO_2. For a significant coupling to occur, two conditions have to be met simultaneously: (a) a strong recoil excitation of rotational degrees of freedom and (b) a notable change in the moment of inertia of the molecule. If the emitter atom is in the center of mass position (C 1s emission), then the rotational oscillators do not receive any recoil energy. Therefore, although the bond length does change upon C 1s emission (as evidenced by the Franck–Condon excitations in the symmetric stretching mode) [39], the condition (a) is not met and the Coriolis coupling does not occur. In the case of O 1s photoemission, there are rotational recoil excitations. Published photoelectron spectra [36, 40] as well as the present spectra show that there is a strong accompanying asymmetric stretching excitation, but no evidence of the symmetric stretching excitations. The exact mechanisms of creating the Franck–Condon vibrational profile were discussed by Domcke and Cederbaum [42], but for the present purposes it is important that upon the O 1s core ionization the C–O^+ bond lengthens by 0.042 Å while the C–O bond shortens by the same amount [40]. In such a case the moment of inertia of CO_2 is affected very little, by about 0.04%, the condition (b) is not met in O 1s photoemission, and the Coriolis coupling corrections are not needed.

The 1s orbitals are isotropic and therefore, even if the photoemission in the laboratory frame is strongly anisotropic, it is still isotropic in the molecular frame (in the HAXPES regime, distortions due to scattering of the outgoing electron on the molecular potential are minor). However, orbitals that are anisotropic in the molecular frame, do result in molecular-frame photoemission anisotropy. The angular averaging when projecting the individual oscillators onto the photoemission axis assumed their isotropic orientations and yielded the coefficients $\frac{1}{3}$ (e.g., equation (7)). Anisotropic emission favoring axial direction of linear molecules would, for example, enhance the recoil contribution of the vibrational oscillators that are related to axial bond stretching. Again, the effects of anisotropy can be incorporated by suitable modifications of the energy fractions f_n.

For the recoil lineshape in the example of CO_2, we used the easily calculable normal modes of the neutral ground state and its accurately known vibrational frequencies. As the geometry and force constants change upon core ionization, the normal mode vectors and frequencies change also. A more accurate recoil lineshape is obtained using values for the particular core-hole state in question which, however, requires considerably more advanced quantum chemical calculations [32]. We tested the model with the vibrational frequencies of the C $1s^{-1}$ and O $1s^{-1}$ core-hole states [43] obtained at the coupled-cluster singles, doubles, and perturbative triples (CCSD(T)) level of theory, using the aug-cc-pvtz basis set [44, 45] and calculated new normal mode vectors for the O $1s^{-1}$ state (for the C $1s^{-1}$ state they are the same as for the ground state, as the $D_{\infty h}$ symmetry is maintained). The recoil lineshapes regenerated with the new values had slightly different σ and μ parameters. A least-squares fit of the O 1s spectra then resulted in a slight improvement (from 1.64 to 1.51) of the χ^2 goodness measure, but the changes in the values of the free fit parameters (widths, Franck–Condon intensity ratios) were less than 1%. It can be therefore concluded, that at least in this example, the additional effort for obtaining more accurate input values for the core-ionized states is not rewarding, since the experimental spectra of polyatomic molecules in general do not reveal sufficient details to support this accuracy.

5. Conclusions

Recoil and Doppler effects in core-level photoemission are conveniently treated as a single phenomenon contributing to the observed photoelectron spectrum. In photoemission from gas-phase polyatomic molecules, we used a model where all degrees of freedom were regarded as independent one-dimensional harmonic oscillators corresponding to the normal modes of the molecule. The photoelectron recoil and the associated Doppler broadening is distributed over these oscillators according to the fraction by which the

motion of the emitter atom contributes to the total kinetic energy in each normal mode. The translational and rotational modes are treated classically, contributing Gaussian-shaped and energy-shifted profiles to the recoil lineshape. The vibrational modes are quantized and, as a result, a significant additional Doppler broadening occurs due to the zero-point motion. That Doppler broadening is manifested as Poisson-distributed excitations of discrete vibrational levels. In the photoelectron spectra of polyatomic molecules, however, the details of these distributions are generally not resolved and we described the total recoil lineshape instead by the first three moments of the recoil-energy distribution function—mean (recoil shift), variance (Doppler broadening) and skewness (effects of the quantization of the vibrational motion). Furthermore, for practical convenience we proposed an approximate function based on translated gamma distribution for describing the recoil lineshape and correctly representing the above characteristics.

Carbon and oxygen 1s photoelectron spectra, measured in tender x-ray regime, we used to test the application of the recoil lineshape on a case where both the detailed, vibrationally resolved analysis and the approximate recoil lineshape analysis can both be reasonably applied, the latter at the lower size limit of its intended target as polyatomic molecules. We showed that the approximate recoil lineshape in its final form, including the Lorentzian core-hole lifetime broadening, gave a very good description of the spectra and that the quantities such as core-hole lifetime and Franck–Condon excitation intensities were extracted accurately, without distortion. On the other hand, neglecting the proper recoil lineshape resulted in major errors in the extraction of such spectroscopic information from the photoelectron spectra.

Lastly, we applied the recoil lineshape model the 1s photoemission by 7 keV photons from the three inequivalent carbons of the pentane molecule and summarized the 'recipe' for using appropriate recoil lineshapes in the analysis of the photoemission spectra from polyatomic molecules of arbitrary size, in the tender x-ray regime.

The recoil lineshape captures all inherent broadenings and energy shifts accompanying the photoemission process, separating it from any purely instrumental contributions and also providing a useful means of accurate energy scale calibration from molecular photoemission lines. The approach can be easily modified to apply to aligned target molecules, molecules adsorbed on surfaces or forming molecular solids. In fact as early as 1976, Flynn considered *phonon broadening* in the x-ray photoemission from solids as a photoelectron recoil effect [46]. A more recent example of an adaptation of the molecular recoil model was presented by Krivosenko and Pavlychev as the *quasi-molecular recoil model* and they suggested that the recoil effects in HAXPES spectra provide a sensitive probe of chemical bonding on surface [13]. Characterization of the recoil lineshapes could lead, for example, to novel ways of characterizing self-assembled monolayers directly from the HAXPES spectra. In such cases, however, one would not expect well-resolved recoil-excited vibrational progressions amenable to a detailed comparison with theory, but rather a general characterization of the recoil envelope in terms of shift, broadening and asymmetry would provide the necessary information.

Acknowledgments

We thank the staff of the GALAXIES beamline at SOLEIL for providing technical support during the remote experiment and T D Thomas for providing quantum chemistry calculations for the core-hole geometries of CO_2 and for scientific advice. EK acknowledges financial support by the Academy of Finland. We acknowledge support by the Open Access Publication Fund of the Freie Universität Berlin.

Data availability statement

The data generated and/or analysed during the current study are not publicly available for legal/ethical reasons but are available from the corresponding author on reasonable request.

Appendix.

Normal mode coordinate displacements and energy fraction coefficients in the CO_2 molecule.

Table A.1. Normal mode coordinate displacements and energy fraction coefficients in the ground-state CO_2 molecule. The last column lists the energy fraction coefficients for the core-hole O $1s^{-1}$ state, obtained from GAUSSIAN calculations [43].

n	Mode	x(O1)	x(C)	x(O2)	y(O1)	y(C)	y(O2)	z(O1)	z(C)	z(O2)	f_n(O)	f_n(C)	f_n(O*)
1	Tsl x	0.5774	0.5774	0.5774	0.0000	0.0000	0.0000	0.0000	0.0000	0.0000	0.3636	0.2727	0.3636
2	Tsl y	0.0000	0.0000	0.0000	0.5774	0.5774	0.5774	0.0000	0.0000	0.0000	0.3636	0.2727	0.3636
3	Tsl z	0.0000	0.0000	0.0000	0.0000	0.0000	0.0000	0.5774	0.5774	0.5774	0.3636	0.2727	0.3636
4	Rot x	0.7071	0.0000	−0.7071	0.0000	0.0000	0.0000	0.0000	0.0000	0.0000	0.5000	0.0000	0.583
5	Rot y	0.0000	0.0000	0.0000	0.7071	0.0000	−0.7071	0.0000	0.0000	0.0000	0.5000	0.0000	0.583
6	Bend x	−0.3314	0.8834	−0.3314	0.0000	0.0000	0.0000	0.0000	0.0000	0.0000	0.1364	0.7271	0.127
7	Bend y	0.0000	0.0000	0.0000	−0.3314	0.8834	−0.3314	0.0000	0.0000	0.0000	0.1364	0.7271	0.127
8	Symm st	0.0000	0.0000	0.0000	0.0000	0.0000	0.0000	0.7071	0.0000	−0.7071	0.5000	0.0000	0.510
9	Asym st	0.0000	0.0000	0.0000	0.0000	0.0000	0.0000	−0.3314	0.8834	−0.3314	0.1364	0.7271	0.053

ORCID iDs

R Püttner https://orcid.org/0000-0002-8761-6873
L Journel https://orcid.org/0000-0001-8044-5437
T Marchenko https://orcid.org/0000-0002-9015-3339
M Simon https://orcid.org/0000-0002-2525-5435

References

[1] Siegbahn K 1982 Electron spectroscopy for atoms, molecules, and condensed matter *Science* **217** 111–21
[2] Condon E U 1928 *Phys. Rev.* **32** 858
[3] Carroll T X, Børve K J, Sæthre L J, Bozek J D, Kukk E, Hahne J A and Thomas T D 2002 *J. Chem. Phys.* **116** 10221
[4] Domcke W and Cederbaum L S 1978 *J. Electron Spectrosc. Relat. Phenom.* **13** 161–73
[5] Sałek P, Gel'mukhanov F, Ågren H, Björneholm O and Svensson S 1999 *Phys. Rev.* A **60** 2786–91
[6] Kukk E *et al* 2005 *Phys. Rev. Lett.* **95** 133001
[7] Fujikawa T, Suzuki R and Kövér L 2006 *J. Electron Spectrosc. Relat. Phenom.* **151** 170–7
[8] Takata Y *et al* 2007 *Phys. Rev.* B **75** 233404
[9] Gel'mukhanov F, Sałek P and Ågren H 2001 *Phys. Rev.* A **64** 012504
[10] Kukk E *et al* 2018 *Phys. Rev. Lett.* **121** 073002
[11] Liu J C, Vaz da Cruz V, Polyutov S, Föhlisch A and Gel'mukhanov F 2019 *Phys. Rev.* A **100** 053408
[12] Krivosenko Y S and Pavlychev A A 2016 *Chem. Phys. Lett.* **664** 233–6
[13] Krivosenko Y S and Pavlychev A A 2013 *Chem. Phys. Lett.* **575** 107–11
[14] Thomas T D 2014 *Phys. Rev.* A **90** 052504
[15] Céolin D *et al* 2019 *Proc. Natl Acad. Sci. USA* **116** 4877–82
[16] Simon M *et al* 2014 *Nat. Commun.* **5** 4069
[17] Céolin D *et al* 2013 *J. Electron Spectrosc. Relat. Phenom.* **190** 188–92
[18] Sekiyama A 2018 Hard x-ray photoelectron spectroscopy *Compendium of Surface and Interface Analysis* ed (Berlin: Springer) pp 229–38
[19] Oura M, Gejo T, Nagaya K, Kohmura Y, Tamasaku K, Journel L, Piancastelli M N and Simon M 2019 *New J. Phys.* **21** 043015
[20] Piancastelli M N, Marchenko T, Guillemin R, Journel L, Travnikova O, Ismail I and Simon M 2020 *Rep. Prog. Phys.* **83** 016401
[21] Drube W 2018 *Synchrotron Radiat. News* **31** 2–3
[22] Rueff J-P, Rault J E, Ablett J M, Utsumi Y and Céolin D 2018 *Synchrotron Radiat. News* **31** 4–9
[23] Schlueter C *et al* 2018 *Synchrotron Radiat. News* **31** 29–35
[24] Samson J A R 1969 *Rev. Sci. Instrum.* **40** 1174–7
[25] Gel'mukhanov F, Ågren H and Sałek P 1998 *Phys. Rev.* A **57** 2511–26
[26] Patanen M, Svensson S and Martensson N 2015 *J. Electron Spectrosc. Relat. Phenom.* **200** 78–93
[27] Sun Y P, Wang C K and Gel'mukhanov F 2010 *Phys. Rev.* A **82** 052506
[28] Thomas T, Kukk E, Ueda K, Ouchi T, Sakai K, Carroll T, Nicolas C, Travnikova O and Miron C 2011 *Phys. Rev. Lett.* **106** 193009
[29] Kukk E *et al* 2017 *Phys. Rev.* A **95** 042509
[30] Suga S and Sekiyama A 2009 *Eur. Phys. J. Spec. Top.* **169** 227–35
[31] Kayanuma Y 2016 Recoil effects in x-ray photoelectron spectroscopy *Hard X-Ray Photoelectron Spectroscopy (HAXPES)* vol 59 ed J Woicik (Berlin: Springer) pp 175–95
[32] Thomas T D *et al* 2008 *J. Chem. Phys.* **128** 144311
[33] Kukk E, Thomas T D and Ueda K 2011 *J. Electron Spectrosc. Relat. Phenom.* **183** 53–8
[34] Thomas T D and Ueda K 2014 *J. Electron Spectrosc. Relat. Phenom.* **195** 101–8
[35] Drahos L and Vékey K 1999 *J. Am. Soc. Mass Spectrom.* **10** 323–8
[36] Kivimäki A, Kempgens B, Maier K, Köppe H M, Piancastelli M N, Neeb M and Bradshaw A M 1997 *Phys. Rev. Lett.* **79** 998–1001
[37] Rueff J-P *et al* 2015 *J. Synchrotron Radiat.* **22** 175–9
[38] Ablett J M *et al* 2013 *J. Phys.: Conf. Ser.* **425** 052007
[39] Carroll T X, Hahne J, Thomas T D, Saethre L J, Berrah N, Bozek J and Kukk E 2000 *Phys. Rev.* A **61** 042503
[40] Hatamoto T *et al* 2007 *J. Electron Spectrosc. Relat. Phenom.* **155** 54–7
[41] Barca G M J *et al* 2020 *J. Chem. Phys.* **152** 154102
[42] Domcke W and Cederbaum L S 1977 *Chem. Phys.* **25** 189–96
[43] Thomas T D 2020 personal communication

[44] Dunning T H 1989 *J. Chem. Phys.* **90** 1007–23
[45] Kendall R A, Dunning T H and Harrison R J 1992 *J. Chem. Phys.* **96** 6796–806
[46] Flynn C P 1976 *Phys. Rev. Lett.* **37** 1445–8